Environ Earth Sci (2015) 73:6891–6898
DOI 10.1007/s12665-015-4414-7

THEMATIC ISSUE

Mathematical modeling of unstable transport in underground hydrogen storage

B. Hagemann[1,2] · M. Rasoulzadeh[2] · M. Panfilov[2] · L. Ganzer[1] · V. Reitenbach[2]

Received: 23 November 2014 / Accepted: 8 April 2015 / Published online: 23 April 2015

Abstract Within the framework of energy transition, hydrogen has a great potential as a clean energy carrier. The conversion of electricity into hydrogen for storage and transport is an efficient technological solution, capable of significantly reducing the problem of energy shortage. Underground hydrogen storage (UHS) is the best solution to store the large amount of excess electrical energy arising from the excessive over-production of electricity, with the objective of balancing the irregular and intermittent energy production, typical of renewable sources such as windmills or solar. Earlier studies have demonstrated that UHS should be qualitatively identical to the underground storage of natural gas. Much later, however, it was revealed that UHS is bound to incur peculiar difficulties, as the stored hydrogen is likely to be used by the microorganisms present in the rocks for their metabolism, which may cause significant losses of hydrogen. This paper demonstrates that besides microbial activities, the hydrodynamic behavior of UHS is very unique and different from that of a natural gas storage.

Keywords Underground hydrogen storage · Displacement instability · Viscous fingering · Lateral gas spreading · Numerical modeling

List of symbols

λ	Pore size distribution index
λ_i	Phase mobility (m^2/Pa/s)
μ	Dynamic viscosity (Pa· s)
ρ	Molar density (mol/m^3)
$\hat{\rho}$	Phase density (kg/m^3)
φ	Fugacity coefficient
ϕ	Porosity
C	Total volume fraction
c	Mole fraction
D	Effective diffusion coefficient (m^2/s)
f	Fugacity (Pa)
g	Gravity acceleration (m/s^2)
H	Henry's law constant (Pa)
J	Diffusive flux (mol/m^2/s)
K	Absolute permeability (m^2)
k_r	Relative permeability
M	Molar mass (kg/mol)
P	Pressure (Pa)
q	Source/sink (mol/m^3/s)
R	Gas constant (J/mol/K)
S	Saturation
T	Temperature (K)
t	Time (s)
u	Total pore velocity (m/s)
v	Darcy velocity (m/s)
x	Vertical dimension (m)

✉ B. Hagemann
birger.hagemann@tu-clausthal.de

[1] Clausthal University of Technology, Clausthal-Zellerfeld, Germany

[2] Laboratoire d'Energétique et de Mécanique Théorique et Appliquée, Université de Lorraine/CNRS, Nancy, France

Introduction

The production of energy from renewable energy sources such as windmills or solar power plants requires temporary storage which is able to balance the irregularities in energy supply and demand. A promising solution is the conversion

of the excess electrical energy into hydrogen gas which will be stored in geological strata (Crotogino et al. 2010). The technology which is called underground hydrogen storage (UHS) comprises electrolyzers, which use the excess electrical energy to split water into hydrogen and oxygen (Kepplinger et al. 2011). The hydrogen is subsequently compressed and injected into the subsurface in suitable geological structures such as depleted gas reservoirs, aquifers, and salt caverns (Roads2HyCom 2008). During periods of low energy production with respect to the demand, the hydrogen gas is withdrawn and reconverted into electricity by the fuel elements or gas-fired turbines, or injected into the network of natural gas and used as fuel in the mixture with methane (Reitenbach et al. 2015). Investigations on the issues of UHS implementing several German UGS as well as impacts of the use and parametrization of the geological subsurface for energy storage are currently being conducted within the framework of the German National joint research projects H2STORE (Ganzer et al. 2013) and ANGUS+ (Bauer et al. 2013; Dethlefsen et al. 2014).

Such a cyclic storage of hydrogen gas is similar to the intermediate storage of natural gas which is needed to maintain the annual balance (Carden and Paterson 1979; Bulatov 1979). However, hydrogen has different characteristics, and its behavior in the subsurface has been insufficiently studied, especially in porous rock formations. Its very low density and low viscosity induce a high tendency for unstable displacement, including gravity overriding and viscous fingering during the injection period (Paterson 1983). The mobility ratio for the displacement of water by hydrogen is in the order of 100 and consequently highly unfavorable. This problem was considered by Paterson (1983), who concluded that in an anticlinal aquifer storage, viscous fingering could spread laterally beyond the spill point and unrecoverable losses of hydrogen could occur. A control parameter for this behavior is the injection rate. During slow hydrogen injection, gravitational forces dominate and stabilize the displacement, while a fast injection leads to the domination of viscous forces and consequently an unstable displacement or viscous fingering. Hence, a limitation on the injection rate could reduce hydrogen losses.

Another problem considered by Panfilov (2010) and Toleukhanov et al. (2012) is the increased activity of microorganisms in the subsurface due to the injection of hydrogen. Hydrogen is a universal electron donor for several microbial species (including archaea and bacteria), which means that it will be metabolized into other substances. Evidence for this phenomenon is given by observations in mixed gas and natural gas storage sites. In the town gas storage site near Lobodice, a drastic change in the gas composition was observed during a storage cycle of 7 months (Buzek et al. 1994). Šmigáň et al. (1990) had observed that an increase in CH_4 and decreases in CO, CO_2 and H_2 resulted from the in-situ production of CH_4 by methanogenic archaea. Also the activity of sulfate-reducing bacteria was observed in several town gas and natural gas storage sites (Kleinitz and Boehling 2005). Several other sources (including Cord-Ruwisch et al. 1988; Lovley and Goodwin 1988) also give hints that acetogenic archeae and iron-reducing bacteria could be stimulated and contribute to the metabolism of hydrogen.

In this paper, a numerical model is presented which is capable of reflecting the hydrodynamic effects of UHS. The model is used to study the injection of hydrogen for storage into a simplified two-dimensional (2D) reservoir, and the results are compared to those obtained from the injection of methane. In addition, the "selective technology" is introduced as a possible solution for the problem of lateral gas spreading. Analytic and numerical results related to this technology are shown for gas rising in a stratified reservoir.

Model of two-phase transport for UHS

The hydrodynamic model is based on the flow and transport of four chemical components: H_2, CO_2, CH_4, H_2O. Numerically, it is implemented using the open source code DuMux developed by the University of Stuttgart.

Governing equations

The mass balance equation is written for each chemical component as follows:

$$\begin{aligned} &\phi \frac{\partial\left(\rho_{\mathrm{g}} c_{\mathrm{g}}^{k} S_{\mathrm{g}}+\rho_{\mathrm{w}} c_{\mathrm{w}}^{k} S_{\mathrm{w}}\right)}{\partial t} \\ &-\nabla \cdot\left(\rho_{\mathrm{g}}\ c_{\mathrm{g}}^{k} v_{\mathrm{w}}+J_{\mathrm{w}}^{k}+\rho_{\mathrm{w}} c_{\mathrm{w}}^{k} v_{\mathrm{g}}+J_{\mathrm{g}}^{k}\right)=q^{k}, \\ &k=\mathrm{H}_2, \mathrm{CO}_2, \mathrm{CH}_4, \mathrm{H}_2\mathrm{O} \end{aligned} \tag{1}$$

where ϕ is the porosity, ρ is the molar density (mol/m^3), c is the mole fraction, S is the saturation, and q the source or sink in (mol/m^3/s). The subscripts g and w denote the gas and water phases, respectively, and the superscript k relates the chemical component.

The fluid velocity v is formulated by Darcy's law:

$$v_i = \lambda_i \cdot (\nabla P_i - \hat{\rho}_i g), \quad i = g, w \tag{2}$$

where P is the phase pressure in (Pa), $\hat{\rho}$ is the phase density in (kg/m^3), and g is the gravity acceleration in (m/s^2).

The phase mobility λ is defined as

$$\lambda_i = \frac{K k_{\mathrm{ri}}}{\mu_i}, \quad i = g, w \tag{3}$$

where k_r is the relative permeability, and μ is the dynamic viscosity in (Pa · s).

The diffusive flux in the gas phase is formulated by the Stefan–Maxwell equation for multicomponent gas mixtures which was simplified using Blanc's law (Poling et al. 2001):

$$J_g^k = \left(\sum_{j=1 \neq i}^{n} \frac{c_g^j}{\rho_g D_g^{ij}} \right)^{-1} \nabla c_g^k \tag{4}$$

where D_g^{ij} is the effective binary diffusion coefficient between component i and component j in (m^2/s).

In the water phase, the diffusive flux is only calculated with respect to H_2O formulated by Fick's law:

$$J_w^k = \rho_w D_w^k \nabla c_w^k \tag{5}$$

where D_w^k is the effective diffusion coefficient of component k in water in (m^2/s).

Closure equations

The system of equations is closed by the sum of saturations:

$$S_g + S_w = 1 \tag{6}$$

and the sum of concentrations:

$$\sum_k c_g^k = 1 \quad \sum_k c_w^k = 1 \tag{7}$$

The capillary pressure and the relative permeability are calculated by the Brooks–Corey correlation (Brooks and Corey 1964):

$$P_c(S_w) = P_g - P_w = P_e S_{we}^{-\frac{1}{\lambda}} \tag{8}$$

$$k_{rw}(S_w) = S_{we}^{\frac{2+3\lambda}{\lambda}} \tag{9}$$

$$k_{rg}(S_w) = (1 - S_{we})^2 (1 - S_{we}^{\frac{2+\lambda}{\lambda}}) \tag{10}$$

where S_{we} is the effective water saturation:

$$S_{we} = \frac{S_w - S_{wr}}{1 - S_{wr} - S_{gr}} \tag{11}$$

where S_{wr} is the residual water saturation, and S_{gr} is the residual gas saturation.

The phases are assumed to be in thermodynamic equilibrium which is determined by the equality of fugacities for each component:

$$f_g^k = f_w^k \quad \text{or} \quad c_g^k \varphi_g^k P_g = c_w^k \varphi_w^k P_w \tag{12}$$

where f is the fugacity in (Pa), and φ is the fugacity coefficient. The gas phase is treated as an ideal gas mixture, and consequently, the fugacity coefficients are set to 1. In the water phase, the coefficients of the gaseous components are calculated using Henry's law:

$$\varphi_w^k = \frac{H^k}{P_w} \tag{13}$$

where H is the Henry's law constant in (Pa). The fugacity coefficient of H_2O is calculated by means of the vapor pressure:

$$\varphi_w^{H_2O} = \frac{P_v^{H_2O}}{P_w} \tag{14}$$

where $P_v^{H_2O}$ is the vapor pressure of pure water in (Pa).

Hydrodynamic parameters

An important influence on the hydrodynamic behavior is due to the phase density and phase viscosity. The gas-phase density is calculated using the ideal gas law:

$$\hat{\rho}_g = \frac{P_g \sum_{k=1}^{4} c_g^k M^k}{RT} \tag{15}$$

where M is the molar mass in (kg/mol), R is the gas constant in (J/mol/K), and T is the temperature in (K). The water-phase density is calculated dependent on the composition by (Class et al. 2002):

$$\hat{\rho}_w = \sum_{k=1}^{4} c_w^k \hat{\rho}^{H_2O} \frac{M^k}{M^{H_2O}} \tag{16}$$

where the density of pure H_2O is constant.

The gas-phase viscosity is calculated by the Wilke method which correlates the viscosity dependent on composition and temperature (Poling et al. 2001):

$$\mu_g = \sum_{i=1}^{4} \frac{c_g^i \mu_g^i}{\sum_{j=1}^{4} c_g^i \omega^{ij}} \tag{17}$$

$$\omega^{ij} = \frac{\left(1 + \sqrt{\frac{\mu_g^i}{\mu_g^j}} \left(\frac{M^i}{M^j}\right)^{\frac{1}{4}}\right)^2}{\sqrt{8\left(1 + \frac{M^i}{M^j}\right)}} \tag{18}$$

where μ_g^i is the viscosity of the pure gas which is correlated using the method of Chung et al., depending on temperature (Poling et al. 2001). The water-phase viscosity is constant.

Numerical implementation

For the numerical implementation, the presented model was transformed into a dimensionless form by using the characteristic parameters of the system. The open source code DuMux was used as the basic framework (Flemisch et al. 2011). DuMux is based on DUNE (Bastian et al.

2008) and was developed for the simulation of multicomponent and multiphase flows and transports in porous media. A 2D unstructured grid is imported in the format of ALUGrid (Dedner et al. 2014). The spatial discretization is done by the Box-method (vertex-centered finite volume method; Helmig 1997). This method is a node-centered finite volume method based on the Galerkin's finite element method. Its advantage compared with finite-volumes and finite-elements is that unstructured grids can be used, while it is also mass conservative.

Simulation study of gas injection into an anticline structure

The simulation study performed in this chapter aims to investigate the lateral spreading of hydrogen compared with methane. Therefore, two different simulation cases were set up. In the first case, hydrogen was injected into a reservoir containing an initial amount of hydrogen, while in the second case, methane was injected into a reservoir containing an initial amount of methane. Each case was simulated at 10 different injection rates, ranging from very low to very high. The characteristic parameters, used in this simulation study, are summarized in Table 1.

The geometry is 2D and represents a vertical slice through an anticlinal structure. The initialization was done by defining the gas–water contact at a certain depth. The phase pressures were calculated using the pressure gradients in hydrostatic equilibrium, and the saturations were related to the capillary pressure by using the Brooks–Corey correlation (Brooks and Corey 1964). The connate water saturation was thereby set to 0.2. The initial gas saturation for the hydrogen case is shown in Fig. 1a. Hydrogen or methane was injected at the top center of the reservoir at a constant rate. The upper and lower boundaries of the reservoir were set to Neumann conditions with no flow across. The left and right boundaries were defined by Dirichlet conditions using the initial values.

Table 1 List of characteristic parameters

Characteristic parameter	Value	Unit
Pressure	6×10^6	Pa
Density	10	kg/m^3
Viscosity	1×10^{-5}	Pa· s
Diffusion coefficient	1×10^{-6}	m^2/s
Length	500	m
Permeability	100	mD
Molar mass	2×10^{-3}	kg
Gravity acceleration	9.81	m/s^2
Time	48.2	days

The interpretation of the simulation results leads to the division into three different displacement regimes which are caused by either the domination of gravitational forces or the domination of viscous forces or their combined action. For low injection rates, the behavior is controlled by gravitational forces. In this case, the gas–water contact lowers evenly and remains horizontal. In Fig. 1b, the gas saturation is shown for the hydrogen case with a dimensionless rate of $\bar{q} = 1 \times 10^{-4}$ after a dimensionless time of $\tau = 108$. No differences were detected in the injection of methane at the same rate.

A different regime was observed for medium injection rates (cf. Fig. 1c, d). In this case, gravitational and viscous forces were influencing the behavior of the gas. The gas–water contact lowered only slightly in the middle part, while the gas spreads laterally below the cap rock. The comparison of Figs. 1c, d indicates that the lateral spreading of hydrogen is faster than that of methane.

For high injection rates, the viscous forces were dominant. Initially the gas–water contact lowered more or less evenly (cf. Fig. 1e). However, the displacement took place at relatively low gas saturation (grey region). Subsequently, the vertical displacement almost stopped, and lateral fingering started to propagate toward the left and right boundaries. Again it could be observed that the lateral spreading of hydrogen was faster than that of methane (cf. Fig. 1f, g).

Selective technology

As shown in the previous chapter, injection of hydrogen induces the problem of unstable displacement. There is a high risk that the injected gas will spread laterally very far and irrecoverable hydrogen could disappear beyond the spill point of the structure. An improvement can be made by injecting the hydrogen at the bottom of the structure. By doing so, the gas rises due to gravitational forces before it arrives below the cap rock. However, when the gas arrives at the top of the reservoir lateral spreading starts to take place in the same way as before and the problem is only delayed by a few days. A possible solution is storage in a reservoir with vertical heterogeneities where the rising of gas will be drastically slowed down. The cyclic operation of hydrogen injection and withdrawal can be achieved by the so-called "selective technology" which is illustrated in Fig. 2.

This concept consists of two systems of wells in a stratified reservoir. The reservoir potentially consists of high porous and high permeable sandstones which are interrupted by thin shale or mudstone layers. The thin layers thereby play the role of horizontal low permeable or even impermeable barriers. One system of wells is used to inject

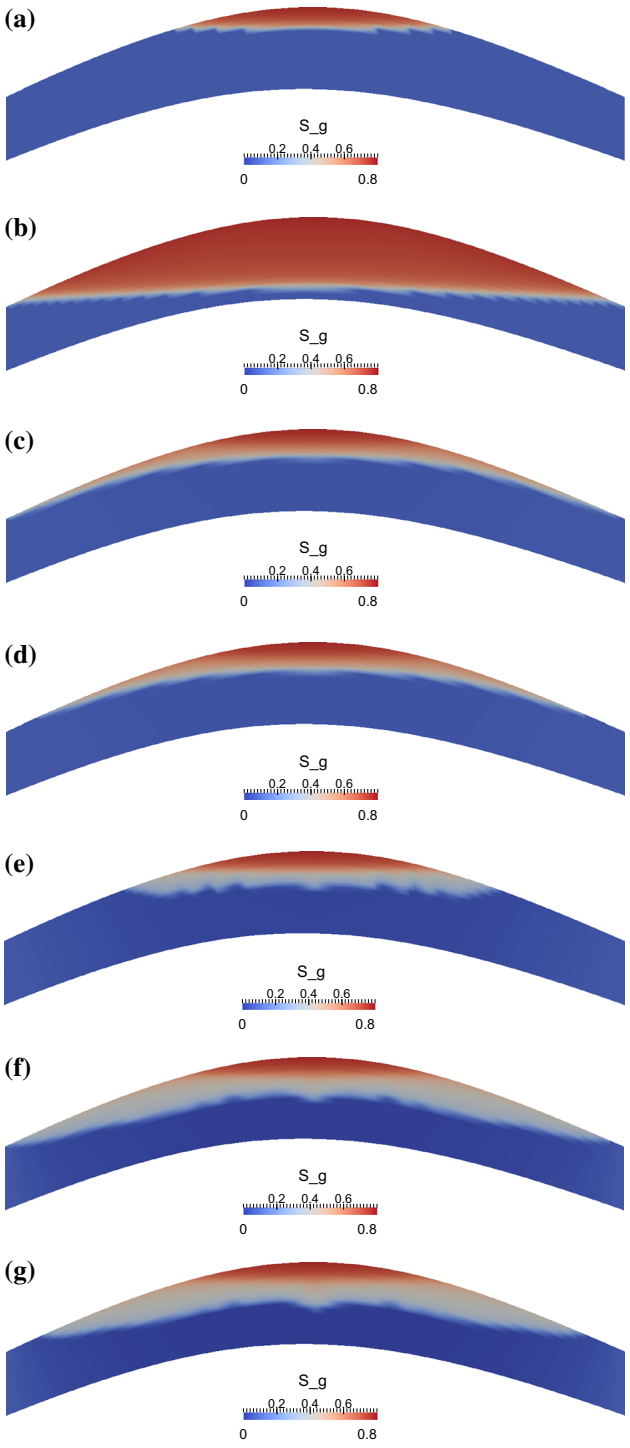

◀**Fig. 1** Numerical simulation of gas injection into the top center of a conceptional two-dimensional anticline structure. **a** Initial gas saturation (S_g). **b** Gas saturation (S_g) after injecting pure hydrogen with a low dimensionless rate ($\bar{q} = 1 \times 10^{-4}$) for a dimensionless time of $\tau = 108$. **c** Gas saturation (S_g) after injecting pure hydrogen with a medium dimensionless rate ($\bar{q}q = 2 \times 10^{-3}$) for adimensionless time of $\tau = 1.04$. **d** Gas saturation (S_g) after injecting pure methane with a medium dimensionless rate ($\bar{q} = 2 \times 10^{-3}$) for adimensionless time of $\tau = 1.04$. **e** Gas saturation (S_g) after injecting pure hydrogen with a high dimensionless rate ($\bar{q} = 0.1$) for a dimensionlesstime of $\tau = 0.05$. **f** Gas saturation (S_g) after injecting pure hydrogen with a high dimensionless rate ($\bar{q} = 0.1$) for a dimensionlesstime of $\tau = 0.128$. **g** Gas saturation (S_g) after injecting pure methane with a high dimensionless rate of ($\bar{q} = 0.1$) for a dimensionlesstime of $\tau = 0.128$

the hydrogen at the bottom of the structure. The hydrogen starts to rise because of the gravitational forces. At the barriers, the vertical migration is retarded until the hydrogen penetrates or flows around. Finally, when the hydrogen arrives at the top of the structure, it will be withdrawn by the second system of wells. It is important to withdraw the hydrogen before it has the chance to spread laterally. However, this method is not common, and its application is

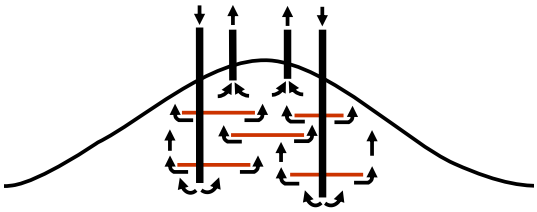

Fig. 2 Sketch of "selective technology": *Red lines* represent low permeable barriers, *arrows* show the flow direction of gas

complex. A detailed planning is required to coordinate the injection rate, withdrawal rate, and time of gas rising. A key element is the selection of a suitable storage site. Once the storage site is constructed, it will only allow for low flexibilities in the storage cycle.

Analytical modeling of gas rising in a stratified reservoir

For the investigation of the "selective technology," the analytical solution was derived for the rising of gas in a stratified reservoir. This required reduction of the geometry to a vertical dimension. The domain was composed of highly permeable intervals with 500 mD, and the barriers were included as low permeable intervals with 250 mD (cf. Fig. 3). It was assumed that the time the gas took to flow through the low permeable barriers was equal to the time it took to flow around the nonpermeable or very low permeable barriers in a two- or three-dimensional case.

The case study analyzed in this chapter assumes that 200,000 Sm^3/day of gas is injected into the bottom of the reservoir. The gas spreads radially up to 100 m and rises equally distributed to the top. The pressure and temperature conditions are defined with 400 bar and 125°C for the calculation of viscosity, density, and phase composition in a two-phase equilibrium. The relative permeability function was again defined by the Brooks–Corey correlation. The system of relations is based on the following assumptions:

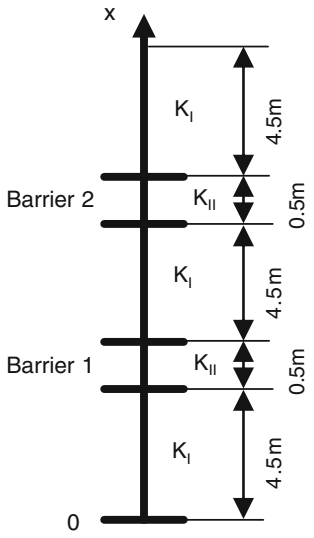

Fig. 3 1D geometry for the analytical solution with high permeable intervals ($K_I = 500$ mD) and low permeable intervals ($K_{II} = 500$ mD)

- Two-phase flow of gas and water
- Incompressible fluids
- No capillary pressure
- No diffusion
- Constant temperature
- Ideal mixing
- Phases in thermodynamic equilibrium

Accordingly, for a system of two components (H_2 and H_2O), it is possible to reduce the transport equations to a unique form:

$$\frac{\partial C^1}{\partial t} + u\frac{\partial F^1}{\partial x} = 0 \tag{19}$$

$$C^1 = c_g^1 S_g + c_w^1(1 - S_g) \tag{20}$$

$$F^1 = \left(c_w^1(1-f) + c_g^1 f\right) + \omega(\hat{\rho}^1 - \hat{\rho}^2)(c_g^1 - c_w^1)(c_w^1 - c_g^1) f k_{rw} \tag{21}$$

$$\omega = \frac{Kg}{\mu_w u \phi} \tag{22}$$

$$f = \frac{\lambda_g}{\lambda_g + \lambda_w} \tag{23}$$

where u is the total pore velocity which is determined by the injection rate.

The initial concentration of H_2 is 0:

$$C^1(t = 0, x > 0) = 0 \tag{24}$$

At the bottom of the reservoir, the concentration of H_2 is set as 1 by a Dirichlet boundary condition which is related to the injection of hydrogen:

$$C^1(x = 0) = 1 \tag{25}$$

The solution of this Riemann problem was obtained by the method of characteristics. Thereby, shocks are constructed by Hugoniot and entropy conditions. The discontinuities at the interfaces between the different permeabilities are constructed by the continuity of fractional flow. A detailed description of the solution technique is planned to be published in a continuing paper. In Fig. 4a, b, the analytical solution is constructed after 0.6 and 0.9 days.

The gas starts to rise with a concentration shock moving upward followed by a rarefaction wave (cf. Fig. 4a). After reaching the first barrier, the profile changes. One concentration shock is moving upward, while a second concentration shock is moving downward, below the first barrier (cf. Fig. 4b). This downward-moving concentration shock represents the increasing accumulation of gas below the barrier and results in a deceleration of the rising velocity. In Fig. 4c, d, the analytical solution is shown after 3 days for two different domains. In Fig. 4c, the domain is periodic which means that the permeability of the second barrier is equal to that of the first one. In Fig. 4d, the domain is nonperiodic whereby the permeability of the second barrier is smaller than the first one.

For both cases, it can be recognized that the upward shock had already reached the top of the domain and the downward shock below the first barrier reached the bottom of the reservoir. For the periodic domain, a downward shock or gas accumulation only occurred below the first barrier. However, for the nonperiodic domain, a second gas accumulation appeared below the second barrier which resulted in a further deceleration of the rising velocity. The analytical solution allowed for the exact determination of the rising velocity. Initially the rising velocity was about 26 times the injection velocity. After passing the first barrier, it had decreased to about 23 times and after passing the second barrier (nonperiodic domain), it had further decelerated to about 16 times the injection velocity.

Numerical modeling of gas rising in a stratified reservoir

A numerical model was implemented to analyze the gas rising in two dimensions. The model was formulated by the mass balance for each component, whereby the flux term was formulated by Darcy's law, and the diffusion was neglected. It contained three components: H_2, CO_2 and H_2O. For simplification, it was assumed that H_2O cannot be present in the gaseous phase, and the concentrations of H_2 and CO_2 in the water phase were estimated by Henry's law. The numerical model was implemented in Comsol Multiphysics and solved implicitly for P, S_g and $c_g^{H_2}$. The

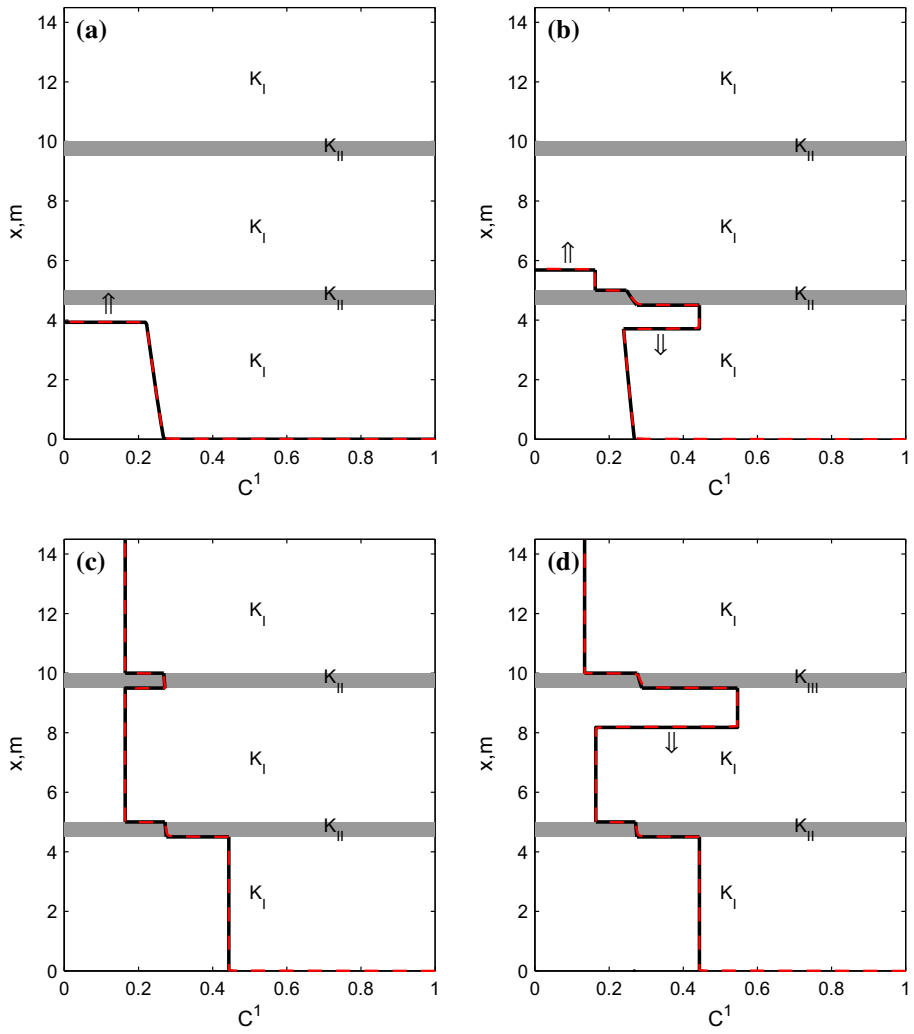

Fig. 4 Analytical solution of hydrogen rising in a stratified reservoir: *white* regions are high permeable ($K_I = 500$ mD), *grey* regions are low permeable ($K_{II} = 250$ mD, and $K_{III} = 125$ mD). **a** Total concentration (see Eq. 20) of H_2in the *vertical dimension* (x) after 0.6 days. **b** Total concentration (see Eq. 20) of H_2in the *vertical dimension* (x) after 0.9 days. **c** Total concentration (see Eq. 20) of H_2in the *vertical dimension* (x) after 3 daysfor a periodic domain (the first and secondbarrier have the same permeability). **d** Total concentration (see Eq. 20) of H_2 inthe *vertical dimension* (x) after 3 days for anon-periodic domain (the second barrier hasa lower permeability than the first one)

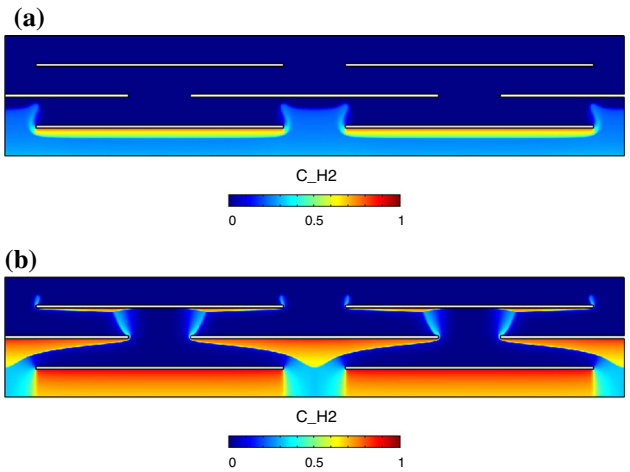

Fig. 5 Numerical simulation of hydrogen rising in a stratified two-dimensional reservoir: *white regions* are impermeable barriers

geometry represents a vertical slice through a simplified reservoir which has a rectangular shape of 100 × 19.5 m. The barriers are impermeable, evenly distributed, and have a dimension of 40 × 0.5 m. The inflow of a mixed gas (95 % H_2 and 5 % CO_2) takes place at the lower boundary at a constant rate. In Fig. 5a, b, the H_2 concentration is shown after 1 and after 4 days.

The results again indicate a delay in the gas rising. Below each barrier, the rising was stopped until the gas has flown around. The gas accumulations below the barriers grew over time as already indicated in the analytical model. Simulations with different spatial dimensions of the barriers showed large differences in the delay in rising. The longer the length, the slower the rising velocity.

Conclusions

– A mathematical model was presented which describes the hydrodynamic effects in UHS. It considers the convective and diffusive fluxes of four chemical components in two mobile phases. Numerically, it is implemented using the open source code DuMux.

- The simulation study of gas injections into a reservoir shows some significant differences depending on the injection rate. For low injection rates, gravitational forces are dominant, and the displacement of water is uniform. However, for higher injection rates, the viscous forces become dominant, and the displacement becomes unstable. Lateral gas fingering starts to propagate below the cap rock toward the left and right boundaries of the reservoir. It has been shown that hydrogen spreads laterally, faster than methane.
- Hydrogen storage in stratified aquifers could prohibit the risk of gas losses due to lateral spreading or viscous fingering beyond the spill point. The implementation requires the "selective technology" whereby the hydrogen is injected at the bottom of the structure and produced below the cap rock. The delay in the gas rising plays a key role in this method.
- The analytical modeling of rising gas shows that downward shocks or gas accumulations occur below the first barrier. A further gas accumulation appears when the second barrier has a lower permeability than the first one. The analytical solution can be used to determine the rising velocity after passing each barrier.
- The numerical model with impermeable but spatial limited barriers also demonstrates the delayed rising of hydrogen. The displaced alignment causes a delay at each line of barriers. The spatial extent of the barriers has a considerable influence on the velocity of the rising gas.

References

Bastian P, Blatt M, Dedner A, Engwer C, Klöfkorn R, Kornhuber R, Ohlberger M, Sander O (2008) A generic grid interface for parallel and adaptive scientific computing. part II: Implementation and tests in DUNE. Computing 82(2–3):121–138

Bauer S, Beyer C, Dethlefsen F, Dietrich P, Duttmann R, Ebert M, Feeser V, Görke U, Köber R, Kolditz O et al (2013) Impacts of the use of the geological subsurface for energy storage: an investigation concept. Environ Earth Sci 70(8):3935–3943

Brooks R, Corey A (1964) Hydraulic Properties of Porous Media. Colorado State University Hydrology Papers, Colorado State University

Bulatov G (1979) Underground storage of hydrogen. PhD thesis, Moscow Gubkin Oil and Gas University (in Russian)

Buzek F, Onderka V, Vančura P, Wolf I (1994) Carbon isotope study of methane production in a town gas storage reservoir. Fuel 73(5):747–752

Carden P, Paterson L (1979) Physical, chemical and energy aspects of underground hydrogen storage. Int J Hydrog Energy 4(6):559–569

Class H, Helmig R, Bastian P (2002) Numerical simulation of non-isothermal multiphase multicomponent processes in porous media.: 1. an efficient solution technique. Adv Water Resour 25(5):533–550

Cord-Ruwisch R, Seitz HJ, Conrad R (1988) The capacity of hydrogenotrophic anaerobic bacteria to compete for traces of hydrogen depends on the redox potential of the terminal electron acceptor. Arch Microbiol 149(4):350–357

Crotogino F, Donadei S, Bünger U, Landinger H (2010) Large-scale hydrogen underground storage for securing future energy supplies. In: 18th World hydrogen energy conference, pp 16–21

Dedner A, Klöfkorn R, Nolte M (2014) The DUNE-ALUGrid module. arXiv preprint arXiv:14076954

Dethlefsen F, Ebert M, Dahmke A (2014) A geological database for parameterization in numerical modeling of subsurface storage in northern gGermany. Environ Earth Sci 71(5):2227–2244

Flemisch B, Darcis M, Erbertseder K, Faigle B, Lauser A, Mosthaf K, Müthing S, Nuske P, Tatomir A, Wolff M et al (2011) DuMu^x: DUNE for multi-{phase, component, scale, physics,...} flow and transport in porous media. Adv Water Resour 34(9):1102–1112

Ganzer L, Reitenbach V, Pudlo D, Panfilov M, Albrecht D, Gaupp R et al (2013) The H2STORE project-experimental and numerical simulation approach to investigate processes in underground hydrogen reservoir storage. In: EAGE Annual Conference & Exhibition incorporating SPE Europec, Society of Petroleum Engineers

Helmig R (1997) Multiphase flow and transport processes in the subsurface: a contribution to the modeling of hydrosystems. Springer, New York

Kepplinger J, Crotogino F, Donadei S, Wohlers M (2011) Present trends in compressed air energy and hydrogen storage in Germany. In: Solution Mining Research Institute SMRI Fall,(2011) Conference. York, United Kingdom

Kleinitz W, Boehling E (2005) Underground gas storage in porous media-operating experience with bacteria on gas quality (spe94248). In: 67th EAGE Conference & Exhibition

Lovley DR, Goodwin S (1988) Hydrogen concentrations as an indicator of the predominant terminal electron-accepting reactions in aquatic sediments. Geochim Cosmochim Acta 52(12):2993–3003

Panfilov M (2010) Underground storage of hydrogen: in situ self-organisation and methane generation. Transp Porous Media 85(3):841–865

Paterson L (1983) The implications of fingering in underground hydrogen storage. Int J Hydrog Energy 8(1):53–59

Poling BE, Prausnitz JM, John Paul O, Reid RC (2001) The properties of gases and liquids. McGraw-Hill, New York

Reitenbach V, Ganzer L, Albrecht D, Hagemann B (2015) Influence of added hydrogen on underground gas storage: a review of key issues. Environ Earth Sci. doi:10.1007/s12665-015-4176-2

Roads2HyCom (2008) Large Hydrogen Underground Storage. www.roads2hy.com

Šmigáň P, Greksak M, Kozánková J, Buzek F, Onderka V, Wolf I (1990) Methanogenic bacteria as a key factor involved in changes of town gas stored in an underground reservoir. FEMS Microbiol Lett 73(3):221–224

Toleukhanov A, Panfilov M, Panfilova I, Kaltayev A (2012) Bio-reactive two-phase transport and population dynamics in underground storage of hydrogen: Natural self-organisation. In: ECMOR XIII-13th European Conference on the Mathematics of Oil Recovery